Journal of Autoimmunity 102 (2019) 77–88

Contents lists available at ScienceDirect

Journal of Autoimmunity

journal homepage: www.elsevier.com/locate/jautimm

Interleukin-1 receptor associated kinase (IRAK)-M -mediated type 2 microglia polarization ameliorates the severity of experimental autoimmune encephalomyelitis (EAE)

Baozhu Liu[a,1], Yong Gu[b,1], Shanshan Pei[a,1], Yu Peng[a], Jinyu Chen[a], Lan V. Pham[c,**], Hai-Ying Shen[d,***], Jun Zhang[e,*], Honghao Wang[a,****]

[a] Department of Neurology, Nanfang Hospital, Southern Medical University, Guangzhou, China
[b] Department of Encephalopathy, Hainan Province Hospital of Traditional Chinese Medicine, Haikou, China
[c] Department of Hematopathology, University of Texas, MD Anderson Cancer Center, USA
[d] Department of Neurobiology, Legacy Research Institute, 1225 NE 2nd Ave, Portland, OR, 97232, USA
[e] Department of Surgical Oncology, University of Texas, MD Anderson Cancer Center, USA

ARTICLE INFO

Keywords:
IRAK-M
Multiple sclerosis
Experimental autoimmune encephalomyelitis
TLR4
Microglia

ABSTRACT

Toll-like receptor 4 (TLR4) play a key role in activating the innate immune system during pathogen recognition. In the pathogenesis of multiple sclerosis (MS), activated TLR4 together with myeloid differentiation primary response gene 88 (MyD88) produce an inflammatory microenvironment that promotes the differentiation of microglia into the M1 phenotype, who plays a key role in the pathogenesis of MS. Interleukin-1 receptor-associated kinase (IRAK)-M is specifically expressed in microglia in central nervous system (CNS) and act as a negative regulator of TLR4-MyD88 signaling pathway. Moreover, previous studies have shown that IRAK-M promotes the differentiation of type 2 microglia; however, its role in MS has not been explored. In the present study, we demonstrated that IRAK-M expression is elevated during EAE, and IRAK-M$^{-/-}$ mice significantly accelerated course and increased severity of disease, accompanied by a visible increase of the M1 microglia infiltrated. In conclusion, these data indicates that IRAK-M significantly improves EAE onset through down-regulation of the TLR4-MyD88 signaling pathway, which finally leads to differentiation of M2 phenotype in the microglia. Our study suggests that IRAK-M may be a potential therapeutic target for the treatment of MS.

1. Introduction

MS is an immune-mediated chronic inflammatory demyelinating disease of the central nervous system (CNS). While the etiology of the disease still remains unknown, it is characterized by multiple demyelinating plaques in the white matter of the central nervous system, with reactive gliosis and axons damage. As MS progresses, microglia and astrocyte are the main infiltrating cells [1,2].

Previous studies have suggested that myelin-reactive CD4 + T helper cell-mediated autoimmunity associated with the inflammatory cascade play an important role in the pathogenesis of MS and EAE, an animal model of MS [3–5]. Myelin-reactive T cells migrate to the CNS, and release cytokines and chemokines to trigger a series of events leading to progressive demyelination [6,7]. In recent years, the important roles of the innate immune system, including microglia, dendritic cells, natural killer cells and mast cells, have also received increasing attention in the initiation or maintenance of inflammation of MS [8]. In particular, microglia, as potentially important innate immune cell in the CNS, is thought to contribute to neurodegeneration in MS and EAE [9–11]. We have reported previously that M2 microglia play protective role in EAE model [12,13]. However, whether IRAK-M can regulate M2 microglia polarization in the CNS or attenuate EAE remain unclear.

* Corresponding author. Department of Surgical Oncology, University of Texas, MD Anderson Cancer Center, 1881 East Rd, Houston, TX, 77054, USA.
** Corresponding author. Department of Hematopathology, University of Texas, MD Anderson Cancer Center, 1515 Holcombe Blvd, Houston, TX, 77030, USA.
*** Corresponding author. Department of Neurobiology, Legacy Research Institute, 1225 NE 2nd Ave, Portland, OR, 97232, USA.
**** Corresponding author. Department of Neurology, Nanfang Hospital, Southern Medical University, 1838 North Guangzhou Avenue, Guangzhou, Guangdong, 510515, PR China.
E-mail addresses: Lvpham@mdanderson.org (L.V. Pham), hshen@downeurobiology.org (H.-Y. Shen), jzhang32@mdanderson.org (J. Zhang), wang_whh@163.com (H. Wang).
[1] These authors have contributed equally to this work.

https://doi.org/10.1016/j.jaut.2019.04.020
Received 31 January 2019; Received in revised form 22 April 2019; Accepted 22 April 2019
Available online 26 April 2019

Activated microglia are divided into two functional subtypes, M1 (classical) and M2 (substitute) phenotypes, which play different roles in the inflammatory process of MS [14,15]. M1 microglia induced by interferon-gamma (IFN-γ), lipopolysaccharide (LPS) or interleukin-17A (IL-17A) is pro-inflammatory and neurotoxic subtype that produces high levels of pro-inflammatory cytokines such as IL-1β, IL-6, IL-12, IL-23, tumor necrosis factor-α (TNF-α) and inducible nitric oxide synthase (iNOS) [16–18]. While, M2 microglia induced by IL-4 or IL-13 is regulatory phenotype, inhibits the immune response and promotes the tissue repair by expressing anti-inflammatory cytokine such as IL-10 [19–21]. On the other hand, M2 microglia can promote Treg response [22].

TLRs are critical pattern recognition receptors (PRRs) that trigger inflammatory signals by sensing unique structural components of both exogenous and endogenous pathogens. TLR4, one of the widely known TLRs, can trigger the MyD88 pathway thereby activates NF-κB and STAT1 signaling, which leads to the production of immune stimulatory cytokines and chemokines. Evolving data have suggested that the activation of TLR4-MyD88 signaling also promotes the M1 microglia polarization [22,23]. There is evidence that TLR4-MyD88 signaling pathway and M1 microglia play important roles in pathogenesis of both MS and EAE [24]. In MS, NF-κB family transcription factors activated through TLR4 pathway, which participated in the development of disease, triggering of recurrence, and regulation of CNS damage [25].

IRAK-M, also known as IRAK-3, is a member of IRAK family, and acts as negative regulator of TLR signaling to prevent excessive inflammation and expressed predominantly in microglia in CNS [26,27]. Studies have shown that IRAK-M prevents the dissociation of the IRAK1-IRAK4 from MyD88 and the activation of the transcription factor NF-κB, thereby down-regulates the release of downstream pro-inflammatory cytokines, such as IL-1β, IL-12 and TNF-α [28]. Moreover, previous studies suggested that IRAK-M$^{-/-}$ mice develop severe osteoporosis and are at higher risk of acute asthma [29,30].

It has been reported that IRAK-M can promote the differentiation of macrophages into M2 in certain disease processes [31]. We further speculate that this regulation of IRAK-M may interfere with the progress of MS/EAE. In the present study, we found that ablation of IRAK-M exacerbated EAE pathology, while over-expressing IRAK-M prevented the progression of EAE. IRAK-M was further found to inhibit the transformation of microglia into M1 phenotype and regulate the transformation of microglia into M2 phenotype by regulating key expression proteins of microglia polarization, such as NF-κB and STAT1.

2. Materials and methods

2.1. Animals

Female C57BL/6 mice (4–6 or 8–10 weeks of age) were purchased from the Experimental Animal Center of Southern Medical University while the IRAK-M$^{-/-}$ mice were obtained from the Jackson Laboratory (Sacramento, CA, USA) and bred freely to standard food and water in a thermostatic room (22 ± 1 °C) under a 12-h light/dark cycle and specific pathogen-free condition. All animal experiments were approved by the Animal Care and Use Committee of the Nanfang Hospital and carried out following the National Institutes of Health Guidelines on the Care and Use of Laboratory Animals.

2.2. EAE induction and monitoring

8-10-week-old female C57Bl/6 mice of the different genotypes and different treatments were immunized subcutaneously with 200 μg myelin oligodendrocyte glycoprotein (MOG)35-55 peptide (MEVGWYRSPFSRVVHLYRNGK) (GL Biochem, shanghai, China) emulsified in complete Freund's adjuvant (containing 4 mg/mL *Mycobacterium tuberculosis*) and injected intraperitoneally with 200 ng pertussis toxin (PTX; Tocris, Bristol, UK) on day 0 and 2. Control animals (CFA) were immunized with the same emulsion without MOG and received pertussis toxinon day 0 and 2. Clinical manifestations of EAE (10 mice per group) were examined daily and last until 30 days after immunization. The clinical scoring criteria for EAE was as follows: 0, no symptoms of disease; 1, decrease of tail tonicity; 2, hind limb weakness or paresis; 3, complete hind limb paralysis; 4, forelimbs and hindlimbs paralysis; 5, dying. Mice were assessed daily for incidence, onset day of disease (At the end of the observation, the day of disease onset of unaffected mice didn't exist and was not used for statistics), time to peak (A score of 3 or greater was defined as the peak of the disease, time to peak referred to the time when the mice reached the peak of the disease after modeling) and peak duration time (referred to the time period during which the mice were at the peak of the disease, mice that did not reach 3 during the observation period were not used for statistics). The assessment was done by a person who was blinded to the genotype/treatment of the mice. Lumbar spinal cords were collected at peak disease for RT-PCR, immunohistochemistry and immunofluorescence analysis.

2.3. Intracerebroventricular (ICV) injection of adeno associated virus serotype 9 (AAV9) vectors in mice

Vector AAV9-IRAK-M and control vector AAV9 were purchased from Hanbio Biotechnology (Shanghai, China). Twenty-six 4-6-week-old WT female mice were randomly divided into two groups with 13 mice in both group: 1) AAV9-IRAK-M group: mice with injection of AAV9-IRAK-M; 2) AAV group: mice with injection of AAV9 (no-load virus). IRAK-M was over-expressed in wide-type (WT) mice by administration of AAV9-IRAK-M (1×10^{11} vg per mouse) vectors 4 weeks before EAE; EAE was then performed with MOG35-55. ICV injections were performed as described before [44]. Briefly, isoflurane (RWD, Shenzhen, China) anesthetized (4% for induction and 2% for maintenance) mice were fixed on the stereotaxic apparatus (RWD, Shenzhen, China) and then excised the skin to expose the bregma. The stereotaxic coordinates of the ICV injection were 1.0 mm on the right side, 0.5 mm on the posterior side of the bregma, and 2.5 mm deep from the dural surface. Four weeks later, EAE was induced, the mRNA expression of IRAK-M was detected by RT-PCR then.

2.4. Histological analysis

Spinal cords were extracted after perfusion of saline and 4% paraformaldehyde, then fixed in 4% paraformaldehyde immediately. After 24 h, the tissues were dehydrated and embedded in paraffin. 5 μm sections were sliced and stained with H&E or LFB for evaluation of inflammation or demyelination as previously described [45]. For immuno-histochemistry, slices were incubated with primary antibodies (iNOS and Arg1, proteintech, Chicago, US) overnight at 4 °C, followed by application of goat against rabbit secondary antibody (ZSGB-BIO, Beijing, China). Images were acquired by light microscopy (Olympus, Tokyo, Japan). The number of inflammatory infiltrating cells of H&E, the number of iNOS or Arg1 positive cells of immunohistochemistry, and the demyelinated region of LFB were calculated in a blinded manner.

2.5. Flow cytometry

Spleen single-cell suspensions and stainings were prepared as previously described [46]. The Leukocyte Activation Cocktail, with BD GolgiPlug™ was used to stimulate splenocytes. For surface staining, cells were incubated with fluorescent antibodies that were specific for CD3, CD4 and CD8 for 30 min at 4 °C. After the cell surface staining procedure, freshly prepared Fix/Perm Buffer was added to each sample and incubated at 4 °C for 40 min protected from light. For intracellular staining, each sample was dispensed into two tubes, one of which was stained with IL-4 and IFN-γ antibodies, the other was stained with IL-17A and FoxP3 antibodies. All reagents for flow cytometry were

purchased from BD Biosciences (San Jose, CA) and used according to the manufacturer's instructions. Analysis was performed using BD LSRFortessa X-20 Cell Analyzer (BD Biosciences, San Jose, CA) and FlowJo software (Treestar, Ashland, OR, USA). Gating strategy was described in supplementary data.

2.6. Primary microglia isolation, culture, and treatment

The isolation of pure primary microglia from mixed glia cultures was carried out as described [47]. Briefly, WT and KO neonatal mice aged between P1—P5 were sacrificed to prepare mixed glial cell population. Fully fused cells cultured in the medium containing DMEM/F12 and 10% fetal bovine serum (FBS, Thermo Fisher Scientific, Waltham,MA) were shaken at 180 rpm for 6 h at 37 °C to collect the microglia. Purified microglia were grown in 6-well or 24-well (with cell slides) plates at a density of 2×10^5 cells/ml for a variety of downstream applications.

The microglia were treated with IFN-γ (100 ng/ml) or IL-4 (10 ng/ml) (Neobioscience, Shenzhen, China) to induce M1/M2 polarization. To elucidate the possible mechanisms by which IRAK-M affects microglia polarization, cells were pretreated with Bay 11-7082 (a specific inhibitor of NF-κB) or fludarabine (a specific inhibitor of STAT1) (Neobioscience, Shenzhen, China) as described [48,49]. The control groups were treated with an equal volume of dimethyl sulfoxide (DMSO). Then IFN-γ and IL-4 were used to induce microglial polarization.

2.7. Immunofluorescence staining

Cells were fixed, permeabilized, blocked, and incubated with primary antibodies against iNOS and Arg1 overnight at 4 °C. The incubation of Alexa Fluor 488-conjugated secondary antibody was followed. DAPI (Boster, Beijing, China) was used to stain the nucleus. Fluorescence images were obtained using the fluorescence microscopy (Olympus, Tokyo, Japan) and the percentage of iNOS or Arg1 positive cells was counted blindly by independent investigators.

2.8. RNA isolation and RT-PCR

Total RNA was isolated from the primary microglia or spinal cords using Trizol (Thermo Fisher Scientific, Waltham, MA). Complementary DNA (cDNA) was synthesized using a PrimeScript RT Master Mix Kit (Takara, Japan) and amplified by RT-PCR using the SYBR Green Real-time PCR Master Mix (Toyobo, Japan) on ABI-Prism 7500 Real-Time PCR System (Applied Biosystems, Carlsbad, CA). The mRNA levels of IL-1β, IL-6, iNOS, IL-10, Arg1, Ym-1, and glyceraldehyde phosphate dehydrogenase (GAPDH) were measured. The expression of mRNA was normalized to the expression of GAPDH. The primer sequences used were as Supplementary Table 1.

2.9. Western blot

Cytoplasmic and nuclear proteins were extracted from the primary microglia and spinal cords using the Minute™ Cytoplasmic and Nuclear Extraction Kit (Invent Biotechnologies, Inc. Beijing, china) according to the manufacturer's protocol. Protease inhibitor cocktail and phosphatase inhibitor (Roche, Basel, Switzerland) were added to the lysis buffer prior to use. Proteins in SDS-loading buffer were separated on a 10% sodium dodecyl sulfate-polyacrylamide gel electrophoresis (SDS-PAGE) and transferred to polyvinylidene fluoride membrane (Millipore, Billerica, MA). After blocking with 5% skim milk powder or bovine serum albumin, the membranes were incubated with primary antibodies against STAT1, p-STAT1, STAT3, p-STAT3, NF-κB P65 (CST, Beverly, MA), iNOS, Arg1, β-actin or TATA binding protein (TBP) (Proteintech, Chicago, US) overnight at 4 °C. Bands incubated with horseradish peroxidase-conjugated secondary antibodies (ZSGB-BIO, Beijing, China) were analyzed using the enhanced chemiluminescence detection method (Millipore, Massachusetts, US). The intensities of protein blots were quantified and normalized to β-actin or TBP using the Image J (National Institutes of Health, Bethesda, MD).

2.10. Statistical analysis

Data were expressed as mean ± SEM. Unpaired two-tailed Student's *t*-test was used to determine statistical significance between the two groups and one-way analysis of variance (ANOVA) with post hoc multiple comparison tests was used to compare continuous data of multiple groups. Kruskal-Wallis test was used to analyze the EAE model. Statistical analyses were performed using GraphPad Prism 6.05 (GraphPad, La Jolla, CA) and SPSS 20.0 (IBM, Armonk, NY, US). $P < 0.05$ was considered statistically significant.

3. Results

3.1. IRAK-M is significantly increased during EAE

We first measured gene expression of IRAK-M in the lumber spinal cord from different groups. The results showed that the level of IRAK-M expression was low in CFA control mice, while the expression of IRAK-M was significantly increased in the EAE mice (Fig. 1 A). To determine the role of IRAK-M in the pathogenesis of EAE, we established both IRAK-M knockout and over-expressing model to observe the clinical sign of EAE. IRAK-M over-expression was induced by injecting adeno-associated virus (AAV) 9-IRAK-M into the lateral ventricles. After 4 weeks, the expression of IRAK-M was detected by RT-PCR. The level of IRAK-M in the IRAK-M group was significantly higher than that in Adeno Associated Virus Serotype 9 (AAV9) group, while the AAV9 group was not different from the WT mice group (Fig. 1 B). This indicates that IRAK-M over-expressing was successful in the IRAK-M group. The levels of IRAK-M were further determined on different groups after EAE modeling. Our data revealed that the level of IRAK-M in over-expressing group was higher than the corresponding AAV9 group, which also confirmed the over-expression of IRAK-M. At the same time, the expression of IRAK-M in the model mice group was significantly higher than that of the corresponding control group (Fig. 1 C).

IRAK-M improves the clinical symptoms and pathological manifestations of EAE.

The clinical scores of different groups were checked daily until 30 days after immunization to assess the effects of IRAK-M on the clinical symptoms of EAE. Our data indicated that the clinical scores of the IRAK-M knockout (KO) mice aggravated, while the over-expressing mice alleviated (Fig. 1 D). Furthermore, we analyzed the incidence, onset time, time to peak and peak duration time of different groups of mice. The results showed that the incidence of IRAK-$M^{-/-}$ mice was higher than that of WT mice, while the incidence of IRAK-M over-expressing mice was lower than that of WT + AAV-con mice (Fig. 1 E). The onset time and time to peak of IRAK-$M^{-/-}$, WT and WT + AAV-con mice were earlier than that of IRAK-M over-expressing mice, meanwhile, the peak duration time of IRAK-M over-expressing mice were shorten than any other group (Fig. 1 **F, G, H**). Moreover, the time to peak of WT and WT + AAV-con mice were delayed compared with that of IRAK-$M^{-/-}$ mice, meanwhile, the peak duration time of IRAK-$M^{-/-}$ mice was significantly extended than that of WT and WT + AAV-con mice, while the over-expressing mice were shortened (Fig. 1 **G, H**).

Histological analysis was performed using the lumbar spinal cords collected at 30 days after immunization. Hematoxylin and Eosin (H&E) staining showed that the number of inflammatory cells was significantly increased after IRAK-M knockout, while decreased in IRAK-M over-expression mice comparing to WT EAE (Fig. 2 **A, C**). Luxol fast blue (LFB) staining was used to assess the loss of myelin in white matter of the lumbar spinal cords. Large loss of myelin was observed in EAE

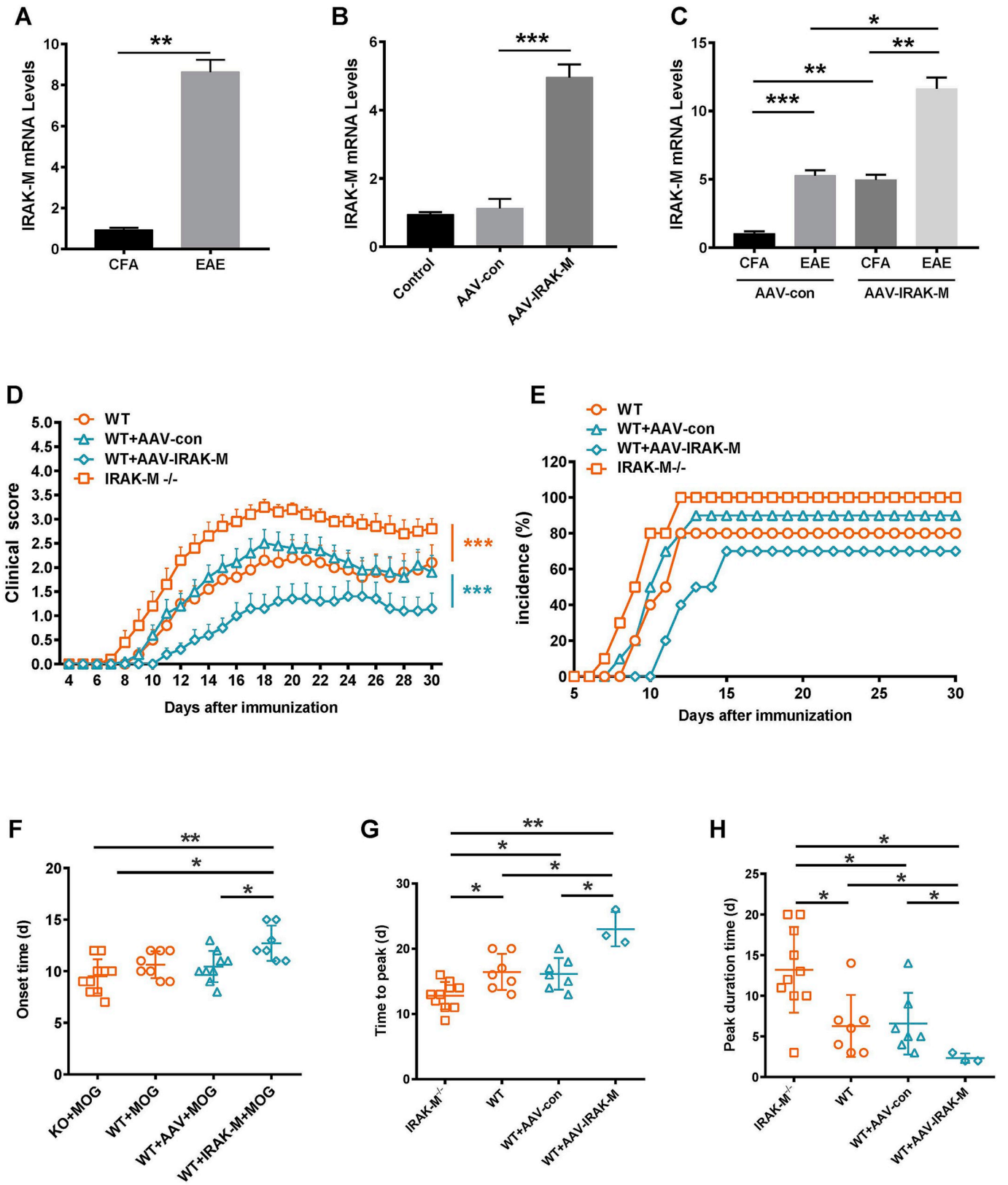

Fig. 1. IRAK-M improves neurobehavioral outcomes in EAE. **(A)** IRAK-M mRNA expression by RT-PCR at peak disease in lumbar spinal cords of WT mice after EAE modeling or CFA controls ($n = 5$). **(B)** IRAK-M mRNA levels were measured in WT, WT + AAV9 and WT + AAV9-IRAK-M mice by RT-PCR before modeling ($n = 3$). **(C)** IRAK-M mRNA levels were measured in WT + AAV9 ($n = 5$) and WT + AAV9-IRAK-M ($n = 5$) mice after EAE modeling. **(D)** Average clinical scores of EAE for each group ($n = 10$). **(E)** Incidence of mice in each group ($n = 10$). **(F)** The onset time of each group of mice ($n = 10$). The onset day of unaffected mice was recorded as 30. **(G)** The time to reach the peak of disease ($n = 10$). A score of 3 or greater was considered to be the peak of the disease. **(H)** The number of days that the peak lasts ($n = 10$). At the end of the observation, the unaffected mouse and the mouse didn't reach peak disease was not counted for statistics in F—H. All the bars represent the mean of measurements from three independent experiments, and the error bars indicate ± SEM. Data are presented as the mean ± SEM. $^{*}P < 0.05$; $^{**}P < 0.01$; $^{***}P < 0.001$.

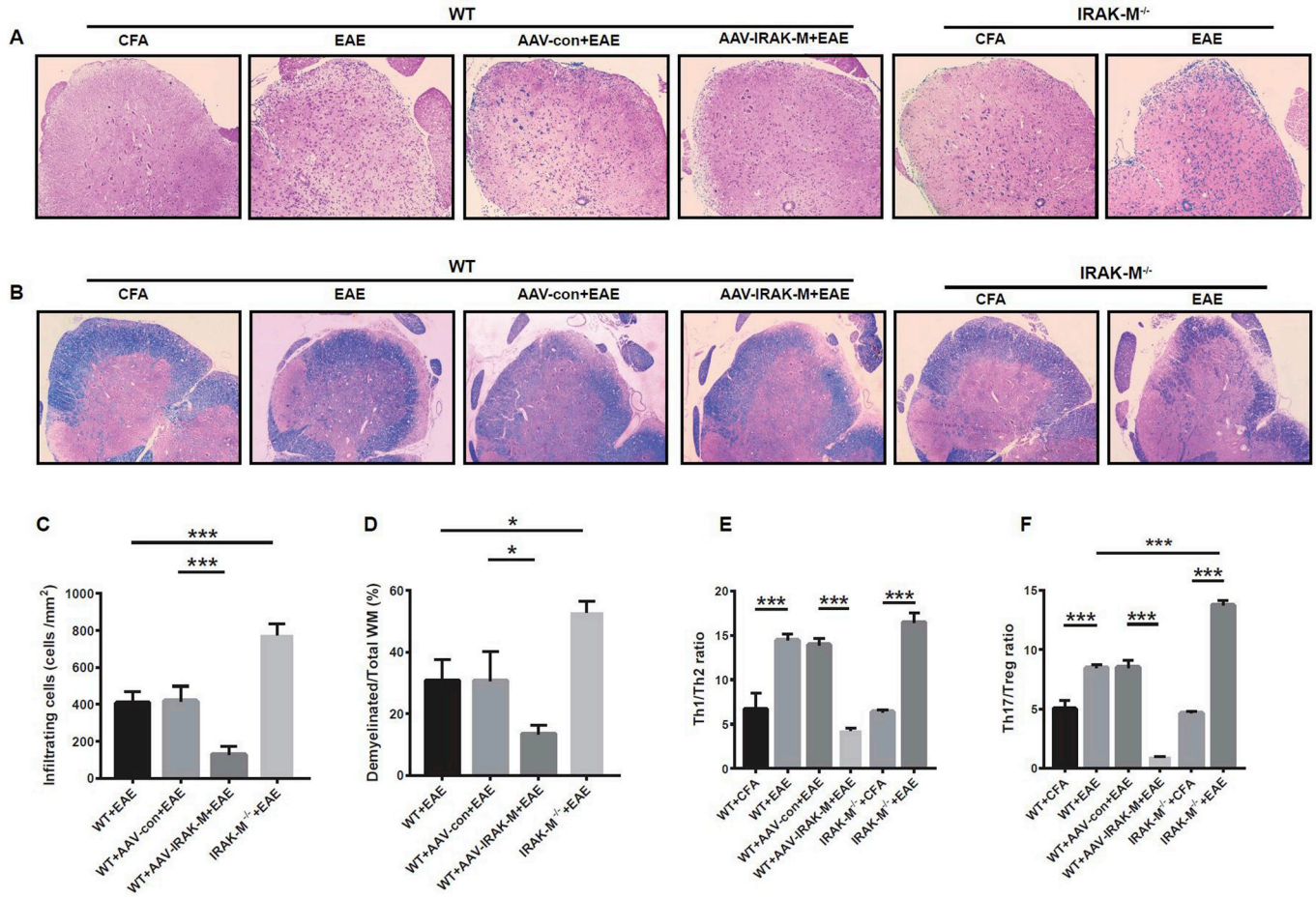

Fig. 2. Ablation of IRAK-M exacerbates inflammation, demyelination, and T-cell axis shift in EAE mice, while over-expression of IRAK-M improve them. Histology analysis of the extent of inflammation and demyelination. **(A)** Representative lumber spinal cord sections of H&E staining (100 ×). **(C)** Histogram showing quantification of the number of infiltrating cells (n = 5 animals per group, three to four fields of view per animal). **(B)** Representative spinal cord sections of LFB staining (100x). **(D)** The percentage of demyelinated white matter (WM) in total WM. Quantification of axonal density was expressed as particles per 10,000 μm^2 (n = 5 animals per group, three to four fields of view per animal). **(E–F)** Flow cytometry analysis of splenocytes. **(E)** Bar graphs showing the changes in the percentages ratio of Th1/Th2 cells. **(F)** The changes in the percentages ratio of Th17/Treg cells. Data are summarized for 4 mice per group. All the above results were measured at peak disease in splenocytes of mice after EAE modeling or CFA controls. All the bars represent the mean of measurements from three independent experiments, and the error bars indicate ± SEM. $*P < 0.05$; $**P < 0.01$; $***P < 0.001$. Error bars indicate SEM.

mice and such situation was exacerbated in the IRAK-$M^{-/-}$ mice, while attenuated in the IRAK-M overexpressing mice (Fig. 2 **B, D**). These results indicated that IRAK-M not only improves the clinical manifestations of EAE, but also improves the pathological manifestations of EAE.

3.2. IRAK-M suppresses pro-inflammatory Th1 and Th17 cells responses

To investigate the possible regulatory immune responses by IRAK-M in vivo, we performed flow cytometry analysis to determine the percentage and number of IFN-γ-producing Th1 cells, IL-4-producing Th2 cells, IL-17A-producing Th17 cells, and $FoxP3^+$ regulatory T (Treg) cells in the spleen. The results showed a significant increase in the ratios of Th1/Th2 and Th17/Treg in the EAE model mice (Fig. 2 **E, F**). Furthermore, the ratios of Th1/Th2 and Th17/Treg in different model groups were compared. The results indicated that the ratios of Th1/Th2 and Th17/Treg in IRAK-M over-expression model mice were decreased (Fig. 2 **E, F**). The ratio of Th17/Treg in KO model mice was significantly higher than that in normal model mice (Fig. 2F), but the ratio of Th1/Th2 was not significantly different (Fig. 2 E). Taken together, these findings suggest that IRAK-M can attenuate the disease severity of EAE by inhibiting Th1 and Th17 cell activation.

IRAK-M promotes M2 polarization of microglia and inhibits M1 polarization in vitro.

We further assessed whether IRAK-M affected the polarization of primary microglia in the CNS. Primary microglia purified from the cerebral cortex of WT or KO mice were stimulated with IFN-γ or IL-4 for 24 h. The further RT-PCR analysis demonstrated that the mRNA levels of IL-1β, IL-6 and iNOS were significantly increased in IRAK-M knockout microglia when IFN-γ was used to induce microglia M1 polarization (Fig. 3 **A**). Whereas in IL-4-induced M2 polarization, the expression of IL-10, Arg1 and Ym-1 in IRAK-M knockout microglia was significantly lower than that of normal microglia (Fig. 3 **B**). In addition, immunofluorescence analysis showed that IRAK-M knockout significantly increased the percentage of iNOS + M1 cells induced by IFN-γ (Fig. 3 **C, E**), while reducing the percentage of IL-4 induced $Arg1^+$ M2 cells (Fig. 3 **D, F**). Collectively, our data clearly demonstrated that IRAK-M promotes M2 polarization of microglia and inhibits M1 polarization in vitro.

3.3. Regulation of IRAK-M expression affects microglia phenotype in EAE mice

Based on the effect of IRAK-M on primary microglia polarization in vitro, we further investigated the effect of IRAK-M on microglia polarization in the EAE model. Immunohistochemistry analysis was used

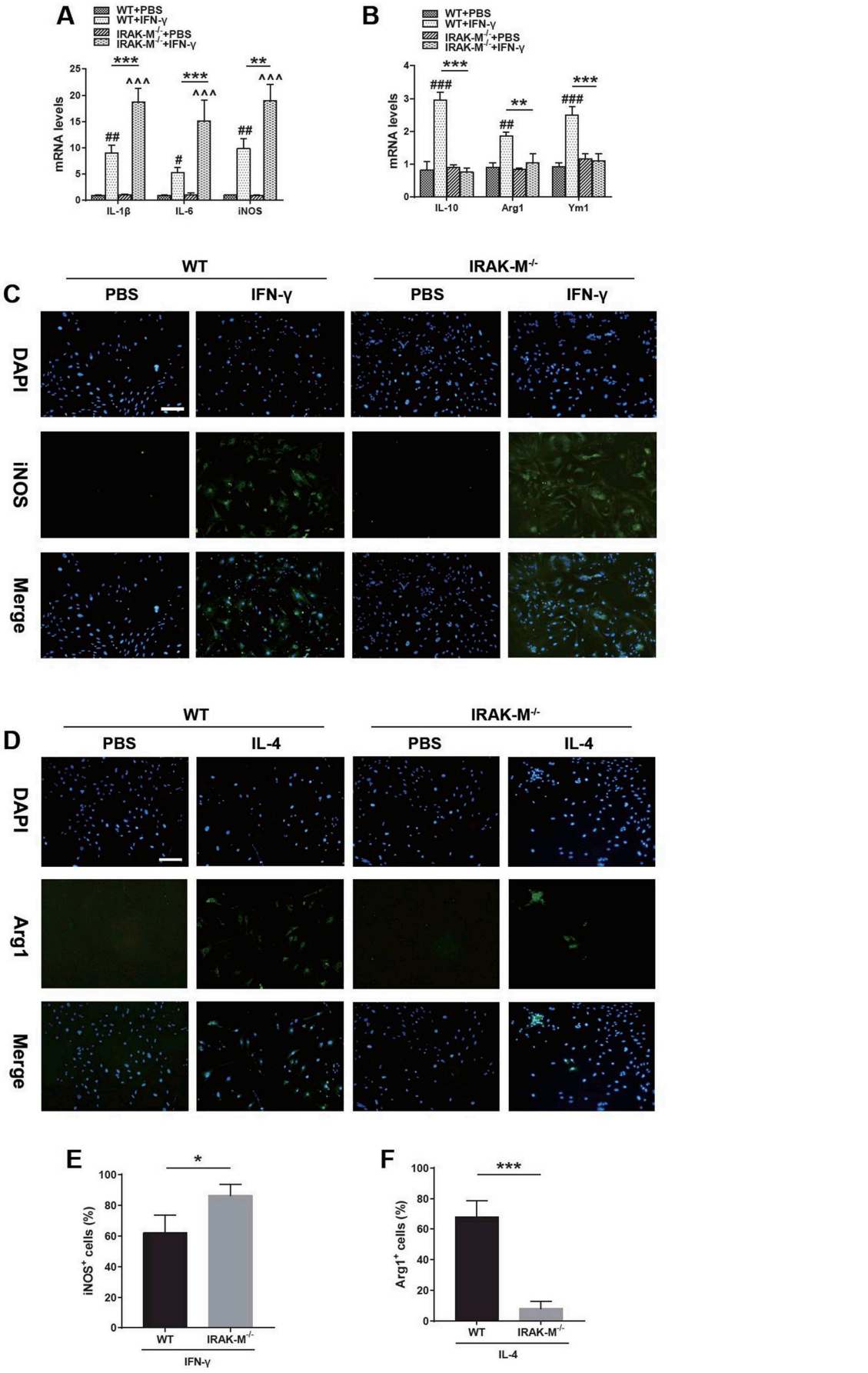

(caption on next page)

Fig. 3. In vitro, IRAK-M deficiency promotes M1 polarization of microglia and inhibits M2 polarization. IFN-γ is used to induce M1 polarization of microglia, and IL-4 is used to induce M2 polarization of microglia. Effects of IRAK-M knockout on the polarization of microglial were demonstrated by detection of M1 polarization markers IL-1β, IL-6 and iNOS **(A)** and M2 polarization markers IL-10, Arg1, and Ym1 **(B)** by RT-PCR. **(C)** IRAK-M knockout or non-knockout microglia were treated with or without IFN-γ for 24 h. Immunostaining for iNOS (green) was performed. DAPI staining is shown in blue (Scale bar = 200 μm). **(D)** Representative images of Arg1 positive M2 cells (green) incubated with the microglia from WT or KO neonatal mice with or without IL-4 stimulation for 24 h. DAPI staining is shown in blue (Scale bar = 200 μm). **(E)** The graph showed the percentage of iNOS positive microglia. **(F)** Percentage of Arg1 positive microglia. Data are the mean ± SEM of three independent experiments. $^{\#}P < 0.05$; $^{\#\#}P < 0.01$; $^{\#\#\#}P < 0.001$ versus WT + PBS mice. $^{\wedge}P < 0.05$; $^{\wedge\wedge}P < 0.01$; $^{\wedge\wedge\wedge}P < 0.001$ versus KO + PBS mice. $^{*}P < 0.05$; $^{**}P < 0.01$; $^{***}P < 0.001$.

to detect the number of iNOS$^+$ M1 and Arg1$^+$ M2 microglia in the spinal cord tissue of different control groups and corresponding EAE groups. We found that M1 and M2 microglia are rare in the normal WT mouse spinal cords. In EAE model, our results showed significant increase number of iNOS$^+$ M1 microglia in IRAK-M$^{-/-}$ mice compared with WT mice, while the number of iNOS$^+$ M1 microglia in IRAK-M over-expressing mice was decreased significantly (Fig. 4 A **line 1, B**). The result of Arg1$^+$ M2 microglia is opposite to that of M1 microglia

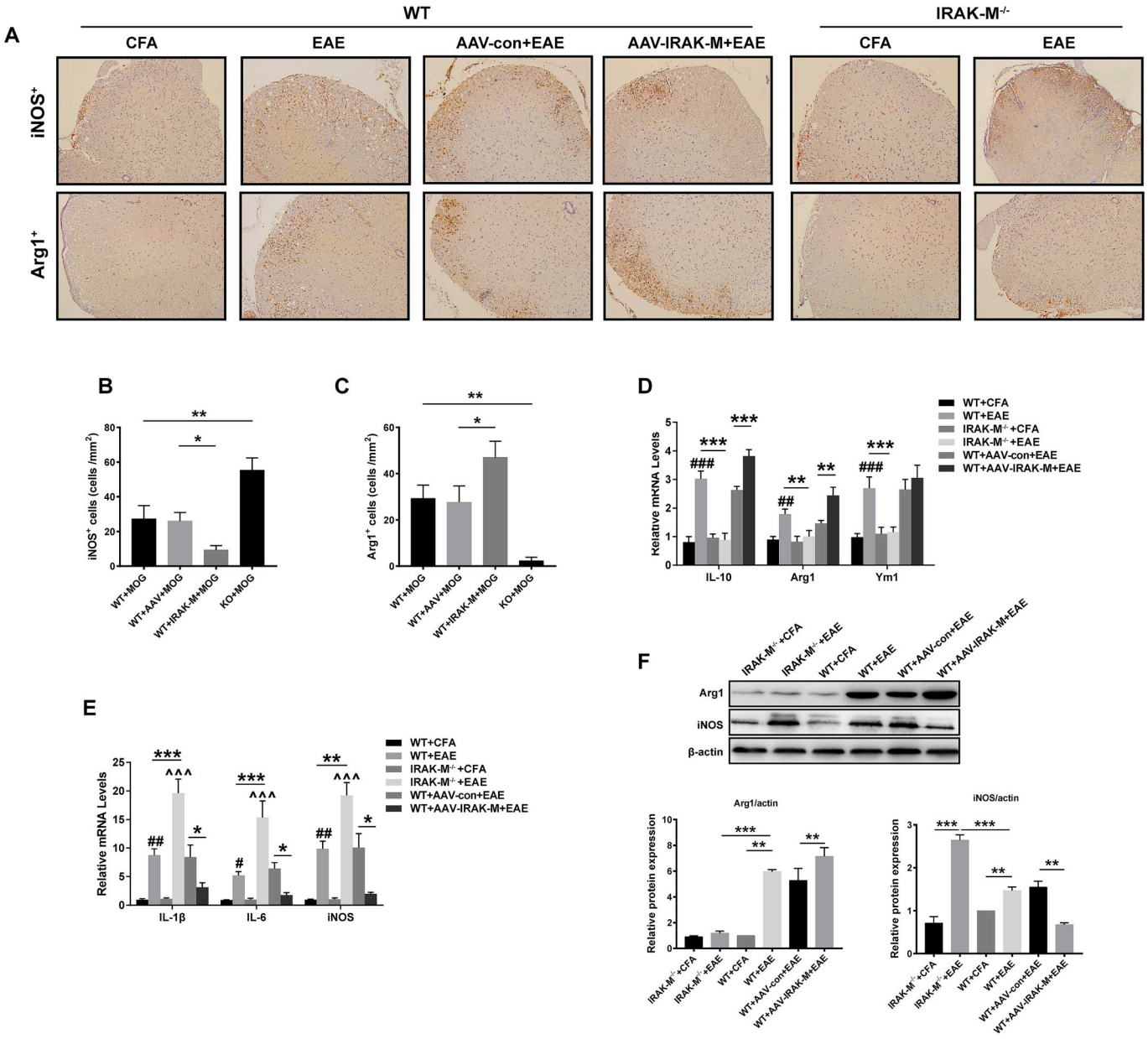

Fig. 4. IRAK-M inhibits M1 polarization of microglia and promotes M2 polarization during EAE. CFA controls and EAE mice of different groups were killed at peak disease and obtained lumbar spinal cords as region of interest. **(A–D)** Immunohistochemistry analysis of the number of M1 and M2 microglia in the lumber spinal cord of mice. **(A)** Representative lumber spinal cord sections of iNOS and Arg1 staining from each group of mice (100 ×). **(B, C)** Histogram showing quantification of the number of iNOS positive cells (M1) and the number of Arg1 positive cells (M2) around lesion sites (n = 5 animals per group, three to four fields of view per animal).**(D, E)** Effects of IRAK-M knockout or over-expression on microglial M1 and M2 polarization. IL-10, Arg1, Ym1 were used as M2 markers. IL-1β, IL-6, and iNOS were used as M1 markers. **(F)** Western blot analysis of Arg1 or iNOS expression in IRAK-M knockout or over-expressing mice. Scanning intensities were quantified and normalized to β-actin. $^{\#}P < 0.05$; $^{\#\#}P < 0.01$; $^{\#\#\#}P < 0.001$ versus WT + CFA mice. $^{\wedge}P < 0.05$; $^{\wedge\wedge}P < 0.01$; $^{\wedge\wedge\wedge}P < 0.001$ versus KO + CFA mice. $^{*}P < 0.05$; $^{**}P < 0.01$; $^{***}P < 0.001$. Data are the mean ± SEM of three independent experiments.

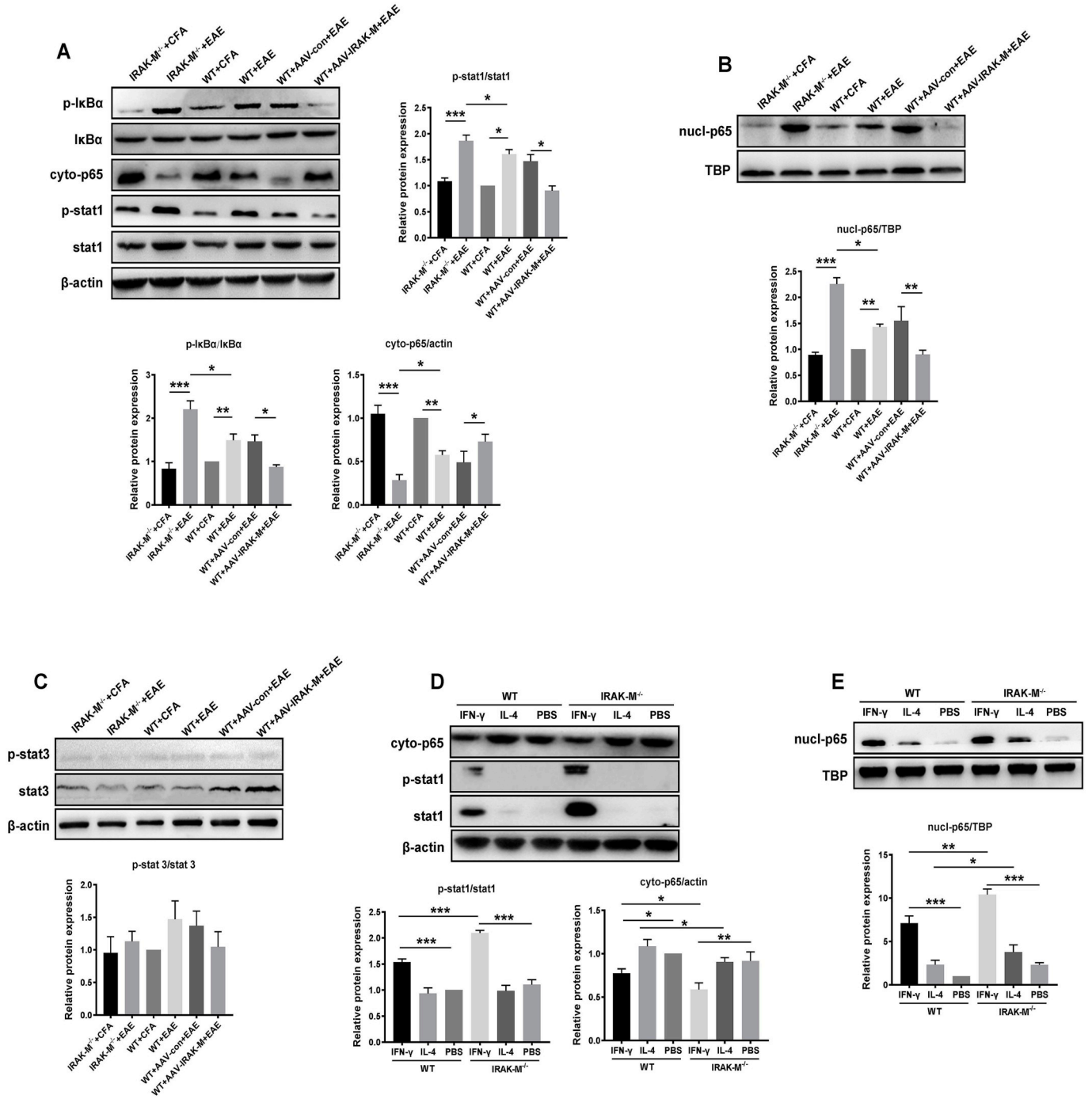

Fig. 5. IRAK-M deficiency enhance nuclear translocation of NF-κB and increase stat1 activity, whereas IRAK-M overexpression results are reversed. Cytoplasmic and nuclear proteins were extracted from the lumber spinal cords (**A-C**) and the cell cultures (**D-E**). (**A**) Representative western blot of stat1, phospho-stat1 (p-stat1), IκBα, p-IκBα and cytoplasmic NF-κB p65 (cyto-p65) is shown. Graphs present the quantification of band intensity for immunoblotting. (**B**) Representative western blot of nucleus NF-κB p65 (nucl-p65) and quantitative protein expression of nucl-p65. **(C)** Representative western blot of stat3 and p-stat3 and quantitative protein expression of p-stat3 based on intensity analysis of Western blot. (**D**) One representative western blot of p-STAT1, total STAT1, and cyto-p65 is shown. (**E**) Representative western blot of nucl-p65. All the bars represent the mean of measurements from three independent experiments, and the error bars indicate ± SEM. $^{*}P < 0.05$, $^{**}P < 0.01$, $^{***}P < 0.001$.

(Fig. 4 A **line 2, C**). Further RT-PCR results showed that the biomarkers of M1 polarization were increased after EAE modeling, and the biomarkers in IRAK-M$^{-/-}$ mice increased more significantly than that in WT mice, while IRAK-M over-expressing mice were decreased (Fig. 4 **E**). For the M2-polarized biomarkers, our data showed that the M2 microglia were increased in WT mice after EAE modeling, and the notable increase in IRAK-M over-expressing EAE mice was more pronounced, while IRAK-M$^{-/-}$ mice were significantly decreased (Fig. 4 **D**). Moreover, western blotting analysis showed that the expression of iNOS was increased in IRAK-M$^{-/-}$ EAE mice and decreased in IRAK-M over-expressing EAE mice, whereas the expression of Arg1 was opposite to iNOS (Fig. 4 **F**). Overall, our results indicated that IRAK-M inhibits the polarization of M1 microglia and promotes polarization of M2 microglia in EAE mice.

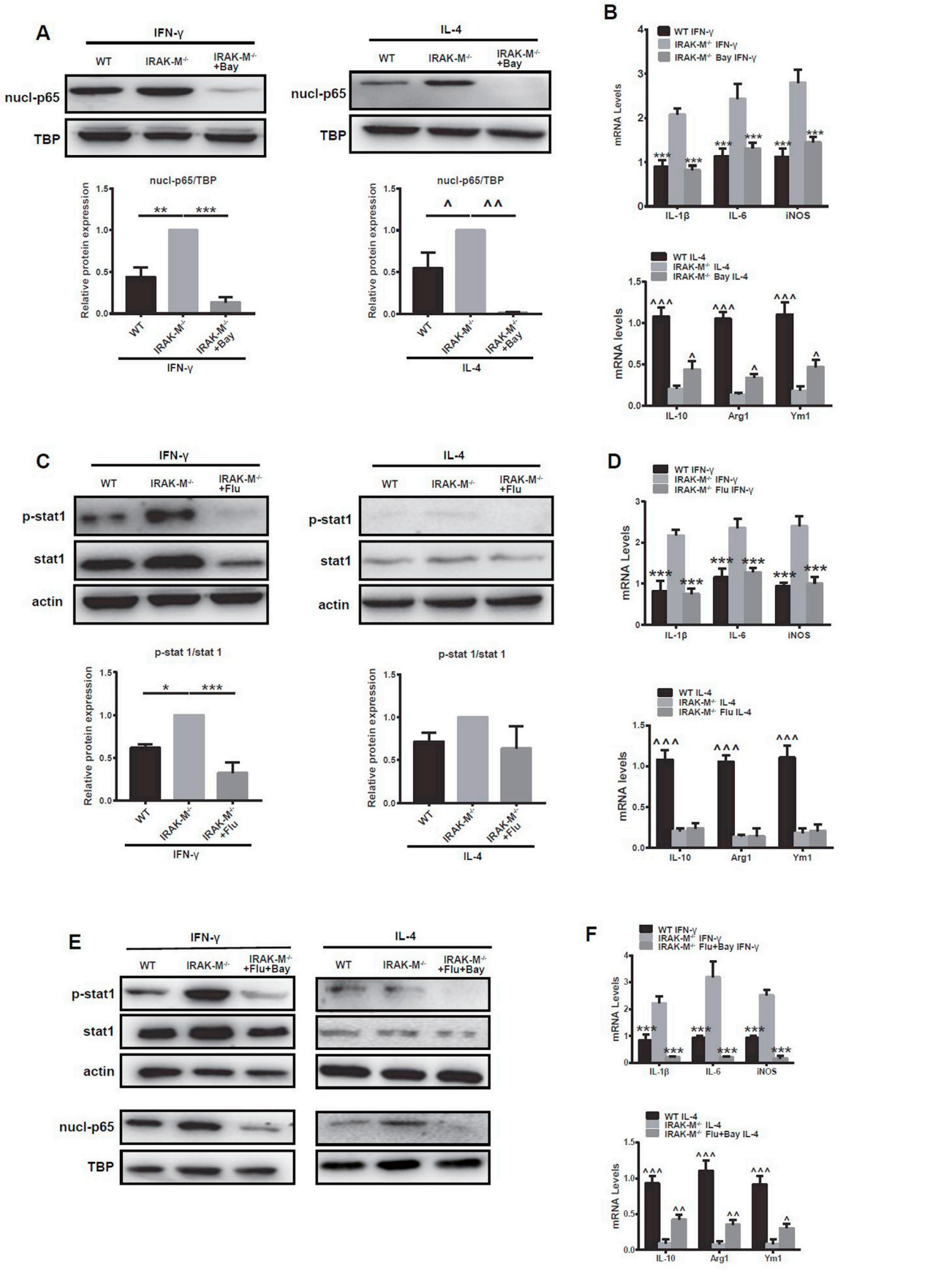

(caption on next page)

Fig. 6. Inhibiting the activation of NF-κB and stat1 inhibit the polarization of M1 and promote the polarization of M2. Bay 11-7082 (Bay, an inhibitor of NF-κB) and fludarabine (Flu, a specific inhibitor of stat1 activation) were used. **(A)** Nucl-p65 was measured by Western blotting. **(B)** Effects of NF-κB inhibition on the polarization of microglial were demonstrated by detecting M1 polarization markers IL-1β, IL-6, iNOS and M2 polarization markers IL-10, Arg1, and Ym1 by RT-PCR. **(C)** STAT1 and p-STAT1 were measured by Western blotting. **(D)** Effects of STAT1 inhibition on the polarization of microglial were demonstrated by detecting M1 polarization markers IL-1β, IL-6, iNOS and M2 polarization markers IL-10, Arg1, and Ym1 by RT-PCR. **(E)** Nucl-p65, STAT1 and p-STAT1 were measured when Bay and Flu are used simultaneously. **(F)** M1 polarization markers IL-1β, IL-6, iNOS and M2 polarization markers IL-10, Arg1, and Ym1 were detected by RT-PCR to determine the effect of simultaneous inhibition of NF-KB and STAT1 on microglia polarization.

3.4. IRAK-M inhibits NF-κB signaling and activation of STAT1

The changes in NF-κB signaling and STAT1 were assessed to delineate the molecular mechanism underlying the observed effects of IRAK-M on microglia. Western blot analysis of spinal cord tissues isolated from EAE mice showed a significant increase in phosphorylated IκB and STAT1, accompanied by an increase in nuclear NF-κB and a decrease in cytosolic NF-κB in KO mice, while not obviously in IRAK-M over-expressing mice (Fig. 5 **A, B**). The phosphorylated STAT3 did not differ significantly between groups of mice (Fig. 5 **C**). Similar results were obtained in vitro with microglia derived from WT or IRAK-M$^{-/-}$ mice. In the process of IFN-γ-induced microglia M1 polarization, phosphorylated STAT1 increased, accompanied by increased nuclear NF-κB and decreased cytosolic NF-κB. The changes in IRAK-M$^{-/-}$ were more obvious (Fig. 5 **D, E**).

Inhibition of NF-κB and STAT1 activation reverses the effect of IRAK-M deletion on microglia polarization.

BAY 11-7082 (Bay) is a NF-κB inhibitor that causes a decrease in nuclear NF-κB by inhibiting phosphorylation of IκBα and activation of NF-κB. Fludarabine (Flu) is an inhibitor of STAT1 that specifically inhibits STAT1 in peripheral blood mononuclear cells. To further verify that IRAK-M affected microglia polarization by inhibiting NF-κB signaling and activation of STAT1, we used Bay to inhibit NF-κB (Fig. 6 **A**), Flu to inhibit STAT1 (Fig. 6 **C**), or inhibit NF-κB and STAT1 simultaneously (Fig. 6 **E**). The RT-PCR results showed that for IFN-γ induced microglia M1 polarization, microglia from IRAK-M$^{-/-}$ mice expressed more M1 markers than that from WT mice (Fig. 6 **B, D, F**). However, after the inhibition of NF-κB or STAT1, the increases of M1 microglia caused by IRAK-M$^{-/-}$ were reversed (Fig. 6 **B, D**). Moreover, the M1 microglia from IRAK-M$^{-/-}$ mice were even less than that from WT mice when both NF-κB and STAT1 had been suppressed (Fig. 6 **F**). For IL-4-induced M2 polarization, it was significantly suppressed in primary microglia from IRAK-M$^{-/-}$ mice when compared with normal primary microglia (Fig. 6 **B, D, F**). Similarly, this inhibition was attenuated when the NF-κB had been inhibited (Fig. 6 **B**). However, inhibition of STAT1 had no effect on primary microglia from IRAK-M$^{-/-}$ mice (Fig. 6 **D**), and inhibition of NF-κB and STAT1 did not differ from inhibition of NF-κB alone (Fig. 6 **F**). Immunofluorescence analysis showed the same results (Fig. 7 **A, B**). These results indicate that IRAK-M affects polarization of M1microglia by affecting NF-κB and STAT1 pathways, whereas IRAK-M affects polarization of M2 microglia only in relation to NF-κB pathway, independent of STAT1 pathway.

4. Discussion

In this study, we explored the anti-inflammatory properties of IRAK-M in the CNS autoimmune diseases. IRAK-M activation was found significantly reduced inflammatory infiltration of the lumber spinal cord and clinical scores in EAE. We further confirmed that the effect of IRAK-M is related to its regulation of microglial polarization. By inhibiting the NF-κB and STAT1 pathways, IRAK-M inhibits M1 microglial polarization and endows them with an M2-like anti-inflammatory phenotype. At the same time, we also found that IRAK-M increased significantly in EAE and specifically reduced the incidence of EAE induced by MOG35–55 and alleviated its clinical symptoms.

Multifocal inflammatory demyelination and degeneration in the CNS white matter are the most important pathological features of MS and EAE, and inhibition of inflammation can reduce the occurrence of demyelination [2]. Previous studies have demonstrated that IRAK-M is involved in the regulation of the inflammatory response by inhibiting the dissociation of IRAK from the transduction complex following activation of the TLR signal [27]. For example, IRAK-M regulates inflammatory responses such as sepsis and influenza infection [32,33]. In IRAK-M$^{-/-}$ mice, inflammation of the intestine induced by *Salmonella typhimurium* can be exacerbated. Furthermore, IRAK-M deficiency leads to an increase in pro-inflammatory cytokines (IL-1β, IL-6 and TNF-α) and expansion of Th1 and Th17 cells, which leads to an increased susceptibility to intestinal inflammation [34]. Our results are consistent with previous. Specifically, IRAK-M over-expressing EAE mice decreased inflammatory response, resulting in lighter clinical manifestations. While in IRAK-M$^{-/-}$ EAE mice, the results are reversed.

IRAK-M also alters the polarity of macrophages and microglia. During M.tb infection, IRAK-M knockdown is shown to promote polarization of macrophage from Ml to M2 phenotype [31]. In addition, Standiford et al. confirmed that tumor-associated macrophages isolated from IRAK-M knockout mice showed characteristics of M1 instead of M2 [35]. Our study confirmed a similar role of IRAK-M in the CNS. Microglia isolated from IRAK-M$^{-/-}$ mice tend to polarize toward M1. M1 microglia inhibit the differentiation of oligodendrocyte progenitor cells into mature oligodendrocytes and the apoptosis of neuronal. In contrast to M1, M2 polarized microglia promote neuronal survival, neurite outgrowth and oligodendrocyte progenitor cell differentiation [18,36–38]. Oligodendrocytes are mainly surrounded on axons of the CNS, forming an insulating myelin structure, assisting in the efficient transfer of bioelectrical signals, and maintaining and protecting the normal function of neurons. Therefore, compared with normal EAE mice, the demyelinating reaction of IRAK-M$^{-/-}$ mice is more severe, while that is alleviated in IRAK-M over-expressing mice.

Activated CD4$^+$T cells are critical in the neuropathology of MS, and CD4$^+$T helper cell subsets interact with M1 and M2 microglia and leads to specific functions and outcomes [36,37]. Primary effector T cells in EAE are Th1 and Th17 cells, whereas disease resolution was promoted by Th2 and Treg cells [39]. M1 microglia create an environment for a Th1 and Th17 reaction [40], while M2 cells can promote Treg response [22]. In addition to its effects on macrophages/microglia, IRAK-M may act directly on inflammatory cells in the periphery, because IRAK-M was found to influence the Th1/Th2 and Treg/Th17 balance and expression of cytokines and chemokines by dendritic cells (DCs) and macrophages during cigarette smoking-induced airway inflammation [41,42]. In the present study, flow cytometric analyses of inflammatory cells from mice spleens revealed decreases in IFN-γ$^+$CD4$^+$ Th1 cells and IL-17A$^+$CD4$^+$ Th17 cells in IRAK-M over-expressing mice. Moreover, splenic Th1 and T17 cells were increased in the IRAK-M$^{-/-}$ mice. These findings suggest that IRAK-M ma attenuate the disease severity of EAE, partly through inhibition of Th1 and Th17 cell infiltration into CNS tissues and splenic Th1 and Th17 cell activation.

Studies have shown that the expression of NF-κB and its downstream factors have a key role in regulating macrophages phenotype [43,44]. M2 polarization induced by astaxanthin can be attenuated by inhibiting NF-κB. STAT family members in the peripheral lymphatic system and CNS regulated the polarization of M1 and M2 during disease progression. IFNs and TLR signaling were promoted by STAT1/NF-κB pathway to slant macrophage to M1 phenotype, whereas M2 phenotype was induced by STAT3 signaling pathway that was activated by IL-4, IL-

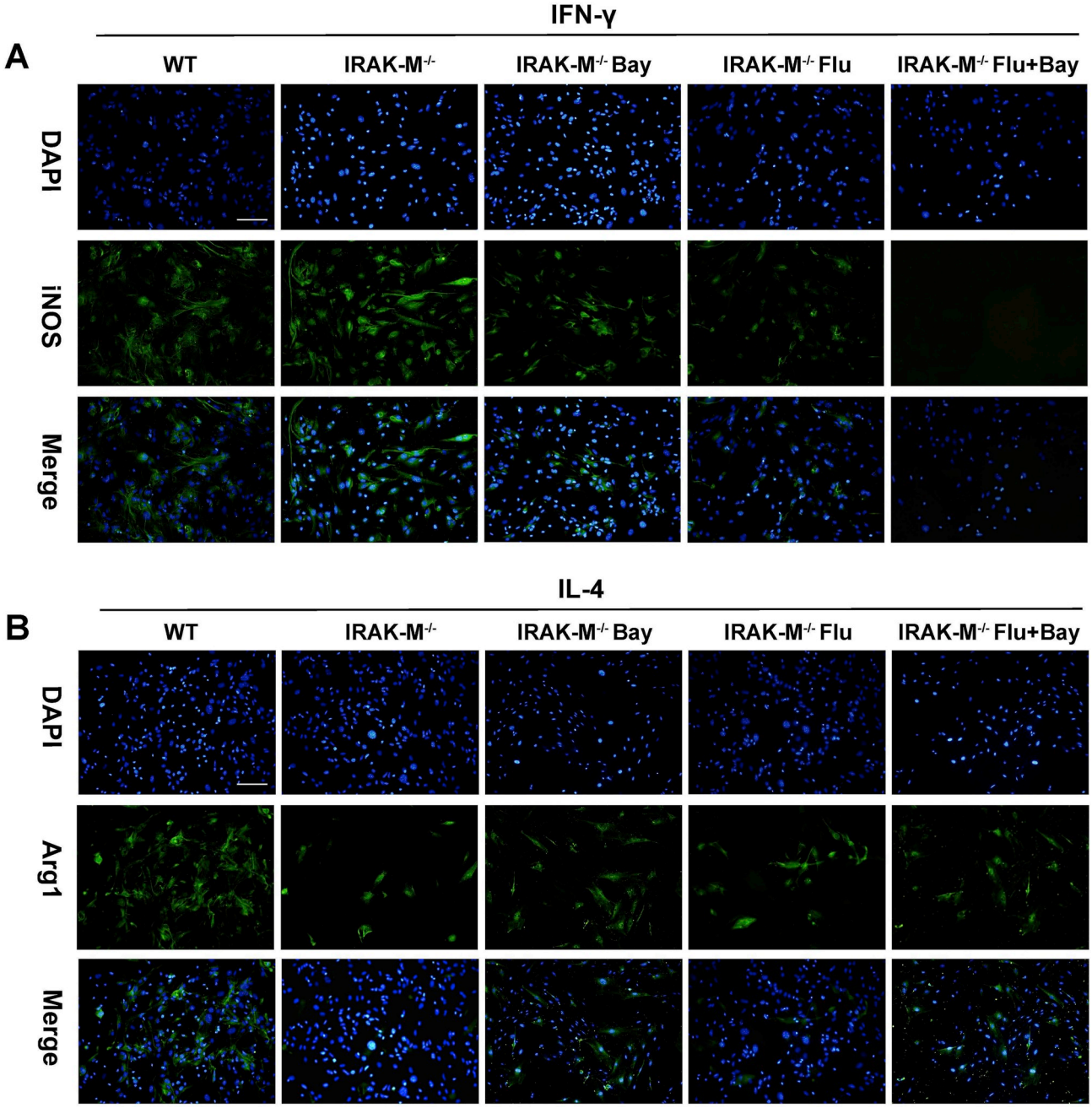

Fig. 7. Immunofluorescence of primary microglia incubated with iNOS or Arg1 primary antibody after treatment of IFN-γ or IL-4. (A)Representative images of iNOS positive M1 cells (green) incubated with the microglia from WT or IRAKM$^{-/-}$ neonatal mice with various treatments. DAPI staining is shown in blue (Scale bar = 200 μm). (B) Representative images of Arg1 positive M2 cells (green) incubated with the microglia from WT or IRAKM$^{-/-}$ neonatal mice with various treatments. DAPI staining is shown in blue. (Scale bar = 200 μm).

10, or IL-13. Our results are consistent with the above conclusions. Animal and cell experiments showed that IRAK-M$^{-/-}$ mice expressed more phosphorylated NF-κB and STAT1, while IRAK-M over-expressing mice expressed less. Moreover, inhibition of NF-κB and STAT1 inhibited the incline of M1 polarization of microglia in IRAK-M$^{-/-}$ Mice. This indicates that IRAK-M inhibit microglia M1 polarization by inhibiting NF-κB and STAT1. Meanwhile, inhibition of NF-κB increased M2 polarization and partially reversed the effect of IRAK-M$^{-/-}$ on M2 polarization, but inhibition of STAT1 did not, suggesting that STAT1 may not participate in this process.

Taken together, we demonstrated that IRAK-M significantly improves the pathogenesis of EAE through inhibiting M1 microglia polarization and promoting of M2 microglia polarization. Our data suggested that IRAK-M may be a potential target for the treatment of MS.

Author contributions

Honghao Wang and Jun Zhang designed experiments and revised the article. Baozhu Liu and Shanshan Pei completed the animal experiments and write the manuscript. Baozhu Liu and Yu Peng completed the cell experiments. Lan Pham revised the article. Jinyu Chen analyzed data and organized pictures. Hai-Hing Shen and Yong Gu provided technical guidances.

Conflicts of interest

The authors declare no conflict of interest.

Acknowledgements

This work was supported by grants from the National Natural Science Foundation of China (No.81673950) and Guangdong Provincial Science and Technology plan projects (No.2016A020215101, 2017A020215182).

Appendix A. Supplementary data

Supplementary data to this article can be found online at https://doi.org/10.1016/j.jaut.2019.04.020.

References

[1] C.A. Dendrou, L. Fugger, M.A. Friese, Immunopathology of multiple sclerosis, Nat. Rev. Immunol. 15 (2015) 545–558.
[2] M. Sospedra, R. Martin, Immunology of multiple sclerosis, Annu. Rev. Immunol. 23 (2005) 683–747.
[3] Y. Komiyama, S. Nakae, T. Matsuki, A. Nambu, H. Ishigame, S. Kakuta, et al., IL-17 plays an important role in the development of experimental autoimmune encephalomyelitis, J. Immunol. 177 (2006) 566–573.
[4] W. Kong, K.M. Hooper, D. Ganea, The natural dual cyclooxygenase and 5-lipoxygenase inhibitor flavocoxid is protective in EAE through effects on Th1/Th17 differentiation and macrophage/microglia activation, Brain Behav. Immun. 53 (2016) 59–71.
[5] J.R. Lees, P.T. Golumbek, J. Sim, D. Dorsey, J.H Russell, Regional CNS responses to IFN-gamma determine lesion localization patterns during EAE pathogenesis, J. Exp. Med. 205 (2008) 2633–2642.
[6] R.A. Hoglund, A.A. Maghazachi, Multiple sclerosis and the role of immune cells, World J. Exp. Med. 4 (2014) 27–37.
[7] L. Legroux, N. Arbour, Multiple sclerosis and T lymphocytes: an entangled story, J. Neuroimmune Pharmacol. 10 (2015) 528–546.
[8] R. Gandhi, A. Laroni, H.L. Weiner, Role of the innate immune system in the pathogenesis of multiple sclerosis, J. Neuroimmunol. 221 (2010) 7–14.
[9] J.F. Bogie, P. Stinissen, J.J. Hendriks, Macrophage subsets and microglia in multiple sclerosis, Acta Neuropathol. 128 (2014) 191–213.
[10] M.T. Fischer, I. Wimmer, R. Hoftberger, S. Gerlach, L. Haider, T. Zrzavy, et al., Disease-specific molecular events in cortical multiple sclerosis lesions, Brain 136 (2013) 1799–1815.
[11] D.Y. Vogel, E.J. Vereyken, J.E. Glim, P.D. Heijnen, M. Moeton, P. van der Valk, et al., Macrophages in inflammatory multiple sclerosis lesions have an intermediate activation status, J. Neuroinflammation 10 (2013) 35.
[12] G. Benedek, J. Zhang, S. Bodhankar, H. Nguyen, G. Kent, K. Jordan, et al., Estrogen induces multiple regulatory B cell subtypes and promotes M2 microglia and neuroprotection during experimental autoimmune encephalomyelitis, J. Neuroimmunol. 293 (2016) 45–53.
[13] G. Benedek, J. Zhang, H. Nguyen, G. Kent, H. Seifert, A.A. Vandenbark, et al., Novel feedback loop between M2 macrophages/microglia and regulatory B cells in estrogen-protected EAE mice, J. Neuroimmunol. 305 (2017) 59–67.
[14] G. Abourbeh, B. Theze, R. Maroy, A. Dubois, V. Brulon, Y. Fontyn, et al., Imaging microglial/macrophage activation in spinal cords of experimental autoimmune encephalomyelitis rats by positron emission tomography using the mitochondrial 18 kDa translocator protein radioligand [(1)(8)F]DPA-714, J. Neurosci. 32 (2012) 5728–5736.
[15] E.M. Chastain, D.S. Duncan, J.M. Rodgers, S.D. Miller, The role of antigen presenting cells in multiple sclerosis, Biochim. Biophys. Acta 1812 (2011) 265–274.
[16] B. Liao, W. Zhao, D.R. Beers, J.S. Henkel, S.H. Appel, Transformation from a neuroprotective to a neurotoxic microglial phenotype in a mouse model of ALS, Exp. Neurol. 237 (2012) 147–152.
[17] A. Mantovani, A. Sica, M. Locati, New vistas on macrophage differentiation and activation, Eur. J. Immunol. 37 (2007) 14–16.
[18] V.E. Miron, A. Boyd, J.W. Zhao, T.J. Yuen, J.M. Ruckh, J.L. Shadrach, et al., M2 microglia and macrophages drive oligodendrocyte differentiation during CNS remyelination, Nat. Neurosci. 16 (2013) 1211–1218.
[19] Z. Jiang, J.X. Jiang, G.X. Zhang, Macrophages: a double-edged sword in experimental autoimmune encephalomyelitis, Immunol. Lett. 160 (2014) 17–22.
[20] B. Luan, Y.S. Yoon, J. Le Lay, K.H. Kaestner, S. Hedrick, M. Montminy, CREB pathway links PGE2 signaling with macrophage polarization, Proc. Natl. Acad. Sci. U. S. A. 112 (2015) 15642–15647.
[21] F.O. Martinez, L. Helming, S. Gordon, Alternative activation of macrophages: an immunologic functional perspective, Annu. Rev. Immunol. 27 (2009) 451–483.
[22] C. Chen, Y.H. Li, Q. Zhang, J.Z. Yu, Y.F. Zhao, C.G. Ma, et al., Fasudil regulates T cell responses through polarization of BV-2 cells in mice experimental autoimmune encephalomyelitis, Acta Pharmacol. Sin. 35 (2014) 1428–1438.
[23] C. Cunha, C. Gomes, A.R. Vaz, D. Brites, Exploring new inflammatory biomarkers and pathways during LPS-induced M1 polarization, Mediat. Inflamm. 2016 (2016) 6986175.
[24] X. Hu, R.K. Leak, Y. Shi, J. Suenaga, Y. Gao, P. Zheng, et al., Microglial and macrophage polarization-new prospects for brain repair, Nat. Rev. Neurol. 11 (2015) 56–64.
[25] S. Miranda-Hernandez, A.G. Baxter, Role of toll-like receptors in multiple sclerosis, Afr. J. Clin. Exp. Immunol. 2 (2013) 75–93.
[26] D.J., G.A. Nicolaes, D. Kruijswijk, M. Versloot, T. van der Poll, V.C. van T, The structure function of the death domain of human IRAK-M, Cell Commun. Signal. 12 (2014) 77.
[27] K. Kobayashi, L.D. Hernandez, J.E. Galan, C.J. Janeway, R. Medzhitov, R.A. Flavell, IRAK-M is a negative regulator of Toll-like receptor signaling, Cell 110 (2002) 191–202.
[28] S. Janssens, R. Beyaert, Functional diversity and regulation of different interleukin-1 receptor-associated kinase (IRAK) family members, Mol. Cell. 11 (2003) 293–302.
[29] L. Balaci, M.C. Spada, N. Olla, G. Sole, L. Loddo, F. Anedda, et al., IRAK-M is involved in the pathogenesis of early-onset persistent asthma, Am. J. Hum. Genet. 80 (2007) 1103–1114.
[30] H. Li, E. Cuartas, W. Cui, Y. Choi, T.D. Crawford, H.Z. Ke, et al., IL-1 receptor-associated kinase M is a central regulator of osteoclast differentiation and activation, J. Exp. Med. 201 (2005) 1169–1177.
[31] P. Shen, Q. Li, J. Ma, M. Tian, F. Hong, X. Zhai, et al., IRAK-M alters the polarity of macrophages to facilitate the survival of Mycobacterium tuberculosis, BMC Microbiol. 17 (2017) 185.
[32] J.C. Deng, G. Cheng, M.W. Newstead, X. Zeng, K. Kobayashi, R.A. Flavell, et al., Sepsis-induced suppression of lung innate immunity is mediated by IRAK-M, J. Clin. Investig. 116 (2006) 2532–2542.
[33] M. Seki, S. Kohno, M.W. Newstead, X. Zeng, U. Bhan, N.W. Lukacs, et al., Critical role of IL-1 receptor-associated kinase-M in regulating chemokine-dependent deleterious inflammation in murine influenza pneumonia, J. Immunol. 184 (2010) 1410–1418.
[34] A. Biswas, J. Wilmanski, H. Forsman, T. Hrncir, L. Hao, H. Tlaskalova-Hogenova, et al., Negative regulation of Toll-like receptor signaling plays an essential role in homeostasis of the intestine, Eur. J. Immunol. 41 (2011) 182–194.
[35] T.J. Standiford, R. Kuick, U. Bhan, J. Chen, M. Newstead, V.G. Keshamouni, TGF-beta-induced IRAK-M expression in tumor-associated macrophages regulates lung tumor growth, Oncogene 30 (2011) 2475–2484.
[36] L. Cao, C. He, Polarization of macrophages and microglia in inflammatory demyelination, Neurosci. Bull. 29 (2013) 189–198.
[37] R. Franco, D. Fernandez-Suarez, Alternatively activated microglia and macrophages in the central nervous system, Prog. Neurobiol. 131 (2015) 65–86.
[38] V.E. Miron, R.J. Franklin, Macrophages and CNS remyelination, J. Neurochem. 130 (2014) 165–171.
[39] J. Goverman, Autoimmune T cell responses in the central nervous system, Nat. Rev. Immunol. 9 (2009) 393–407.
[40] T. Krausgruber, K. Blazek, T. Smallie, S. Alzabin, H. Lockstone, N. Sahgal, et al., IRF5 promotes inflammatory macrophage polarization and TH1-TH17 responses, Nat. Immunol. 12 (2011) 231–238.
[41] H. Gong, T. Liu, W. Chen, W. Zhou, J. Gao, Effect of IRAK-M on airway inflammation induced by cigarette smoking, Mediat. Inflamm. 2017 (2017) 6506953.
[42] D.E. Rothschild, Y. Zhang, N. Diao, C.K. Lee, K. Chen, C.C. Caswell, et al., Enhanced mucosal defense and reduced tumor burden in mice with the compromised negative regulator IRAK-M, EBioMedicine 15 (2017) 36–47.
[43] H. Zhou, M. Yu, K. Fukuda, J. Im, P. Yao, W. Cui, et al., IRAK-M mediates Toll-like receptor/IL-1R-induced NFkappaB activation and cytokine production, EMBO J. 32 (2013) 583–596.
[44] F. Zhang, Y. Xuan, J. Cui, X. Liu, Z. Shao, B. Yu, Nicorandil modulated macrophages activation and polarization via NF-kappab signaling pathway, Mol. Immunol. 88 (2017) 69–78.
[45] J. Zhang, A. Lapato, S. Bodhankar, A.A. Vandenbark, H. Offner, Treatment with IL-10 producing B cells in combination with E2 ameliorates EAE severity and decreases CNS inflammation in B cell-deficient mice, Metab. Brain Dis. 30 (2015) 1117–1127.
[46] J. Zhang, Z. Huang, R. Sun, Z. Tian, H. Wei, IFN-gamma induced by IL-12 administration prevents diabetes by inhibiting pathogenic IL-17 production in NOD mice, J. Autoimmun. 38 (2012) 20–28.
[47] M. Djelloul, N. Popa, F. Pelletier, G. Raguenez, J. Boucraut, RAE-1 expression is induced during experimental autoimmune encephalomyelitis and is correlated with microglia cell proliferation, Brain Behav. Immun. 58 (2016) 209–217.
[48] W. Li, J. Yi, X. Zheng, S. Liu, W. Fu, L. Ren, et al., miR-29c plays a suppressive role in breast cancer by targeting the TIMP3/STAT1/FOXO1 pathway, Clin. Epigenet. 10 (2018) 64.
[49] K.S. Kirkley, K.A. Popichak, M.F. Afzali, M.E. Legare, R.B. Tjalkens, Microglia amplify inflammatory activation of astrocytes in manganese neurotoxicity, J. Neuroinflammation 14 (2017) 99.